Preparation and Properties of Wear-Resistant Carbonized-Ceramic Composite Coating on Pure Aluminum Surface

Zhonglei Shao [1], Lu Chen [2, *], Hailin Lu [2], and Fulin Fan [1, *]

[1] Institute for Energy and Environment, University of Strathclyde, Glasgow, G1 1XW, United Kingdom

[2] Group of Mechanical and Biomedical Engineering, College of Mechanical and Electronic Engineering, Xi'an Polytechnic University, Xi'an, Shaanxi, 710048, PR China.

Corresponding Authors: F. Fan (f.fan@strath.ac.uk), L. Chen (821945275@qq.com)

Abstract

In this paper, a new composite coating was prepared on the surface of pure aluminum (Al) by combining the micro-arc oxidation (MAO) technology with the polyethylene glycol (PEG 400) carbonization technology. The composite coating and the single MAO coating were observed by scanning electron microscope (SEM) and energy-dispersive spectrometer (EDS), finding that the single MAO coating surface with volcano-like pores and microcracks was covered by the carbonized layer of the composite coating where the overall coating thickness was around 19.5 μm including 17.5 μm of inner MAO coating. The material properties of the composite coating were characterized by X-ray diffraction (XRD) and X-ray photoelectron spectroscopy (XPS). The wear resistance of the composite coating was tested under dry friction conditions, finding that the wear width on the composite coating surface was 909.6 μm only, which was around 55.7%, 50.4% and 58.2% of those for pure Al substrate, single carbonized coating and single MAO coating respectively. Then the comprehensive wear resistance of the composite coating was explored under different sliding speeds and lubrication mediums. Finally, the wear-resisting mechanism of the composite coating was discussed, concluding that the composite coating could effectively reduce adhesive wear and abrasive wear of the Al substrate.

Key words: Aluminum, Composite coating, Micro-arc oxidation (MAO), Polyethylene glycol (PEG 400) carbonization, Wear resistance

1. Introduction

Aluminum (Al) is favored by design and manufacturing industries due to its abundant production, light weight, easy processing and good corrosion resistance, especially in electric cables, aviation, construction and automotive fields. However, the disadvantages of pure Al such as wear resistance, low hardness and easy deformation constraint the use of pure Al and make it difficult to provide the required mechanical properties of the products. [1, 2] Therefore, the surface modification of pure Al is required to meet the product requirements, so as to achieve a wider range of application.

A large number of treatment methods are available for material surface modification, such as the micro-arc oxidation (MAO), [3-5] anodic oxidation, [6-8] chemical vapor deposition, [9, 10] physical vapor deposition, [11, 12] electroplate, [13, 14] surface carbonization, [15, 16] etc. The MAO technology is a surface modification means of using high-voltage discharge to form an electric arc spark, which in turn penetrates the surface

This is a peer reviewed, accepted author manuscript of the following journal article: Shao, Z., Chen, L., Lu, H., & Fan, F. (2022). Preparation and properties of wear-resistant carbonized-ceramic composite coating on pure aluminum surface. International Journal of Applied Ceramic Technology. https://doi.org/10.1111/ijac.14224

of the metal and grows the corresponding metal oxides in situ. It is mainly applied to Al, Mg, Ti metals and corresponding alloys, improving the resistance of metal surfaces to wear and corrosion. [17] Zhang et al. treated 7N01 Al alloys with the MAO technology and generated the Al oxide ceramic coating in-situ on the surface, which improved the wear resistance and corrosion resistance of the coating over the Al alloy substrate. [18] The choice of electrolyte and the setting of parameters in the MAO process have a great influence on the coating. The electrolyte systems commonly employed by the MAO method are phosphate, silicate and aluminate systems. It has been experimentally confirmed that the coating prepared by the aluminate system is more dense and wear-resistant, [19, 20] while the silicate system can accelerate the growth of the coating and the phosphate system can accelerate the discharge of the medium to promote the coating generation. [21] The parameters of the MAO process mainly comprise current density, frequency, duty cycle and time, which influence the quality of the MAO coating formed. Liu et al. conducted MAO experiments by altering the current density with the other parameters as control quantities, and found that the surface morphology, thickness and corrosion resistance of MAO coatings significantly changed with an increasing current density. [22] The surface carbonization technology is another means of metal surface modification, which coats the metal surface with a layer of carbonizing agent and then carbonizes the surface by heating. This will form a thin layer of carbonized film on the metal surface, which can effectively enhance the wear resistance of the metal substrate. Li et al. used the gradient heating to carbonize the bearing steel surface, which formed the graphene oxide/polyethylene glycol (GO/PEG) composite lubricant and effectively reduced the wear situation of the metal substrate surface. [15] The carbonized coating is largely affected by the choice of carbide and the control of temperature. The carbide is generally selected based on the product requirement, and then the temperature is set according to the properties of the carbide adopted. The polymer containing carbon or the graphene-like substance is usually employed as the carbide in order to improve the wear resistance of the metal surface. [15, 16]

The MAO and surface carbonization technologies can effectively reduce the wear of the Al substrate. However, the MAO coating surface containing micropores and microcracks has a high roughness which, together with the high hardness and brittleness of the coating, can make it suffer from severe plastic deformation (abrasive wear) under high load, resulting in poor wear resistance. In addition, the PEG-carbonized coating is easy to fall off from the Al substrate under high load due to it poor bonding strength and low hardness. The contribution of this paper is to combine the two technologies and measure their combined effects on the improvement of wear resistance of pure Al. The surface of pure Al substrate was first treated by the MAO method, and then carbonized to generate a composite coating. The surface of the composite coating was observed by the scanning electron microscope (SEM), and its material properties were analyzed by using the X-ray diffraction (XRD), X-ray photoelectron spectroscopy (XPS) and energy-dispersive spectrometer (EDS) respectively. Furthermore, the wear resistance of the composite coating was verified through tribological tests, based on which the wear resisting mechanism was investigated.

2. Experimental Details

2.1. Materials

Sodium hexametaphosphate ($(NaPO_3)_6$), sodium hydroxide (NaOH), ammonium metavanadate (NH_4VO_3), sodium chloride (NaCl), sodium silicate (Na_2SiO_3), sodium tungstate (Na_2WO_4), polyethylene glycol (PEG, molecular weight: 4000) and PEG (molecular weight: 400) were purchased from Tianjin Damao Chemical Reagent Factory (Tianjin, China). All reagents were of analytical purity (AR).

2.2. Composite coating preparation

In the MAO process, the bipolar MAO power supply (FL7-MAOB60A, Xi'an Juncheng Precision Technology Co. LTD, China) was used, and the electrolyte was configured based on the materials and their concentrations listed in Table 1. The pure Al disk was polished on 500#, 1000#, 2000# and flannel in sequence, and placed in an acetone bath and ultrasonically cleaned for 30 min. Then the Al disk was connected to the positive electrode of the bipolar MAO power supply, while the negative electrode was placed in the electrolyte. Throughout the MAO process, the cooling system was switched on given the MAO parameters listed in Table 2. At the beginning of the MAO process, as shown in Fig. 1-I, the MAO power supply, electrolyte and MAO coating formed a complete closed loop. After 10 min, the MAO coating was produced, with its quality being closely related to the concentration of electrolyte. In the following carbonization process, 0.5(±0.1) mL PEG 400 was added onto the MAO coating, which was then put in a muffle furnace and heated at 300°C for 2 h, as shown in Fig. 1-II, eventually forming the composite coating.

Table 1. Electrolyte materials and concentrations.

Material	Concentration (g/L)
$(NaPO_3)_6$	28
NaOH	2
Na_2SiO_3	3
Na_2WO_4	5
NH_4VO_3	8
PEG 4000	1

Table 2. MAO process parameters

Parameter	Frequency (Hz)	Current density (A/dm^2)	Duty cycle (%)	Oxidation time (min)
Value	600	10	20	10

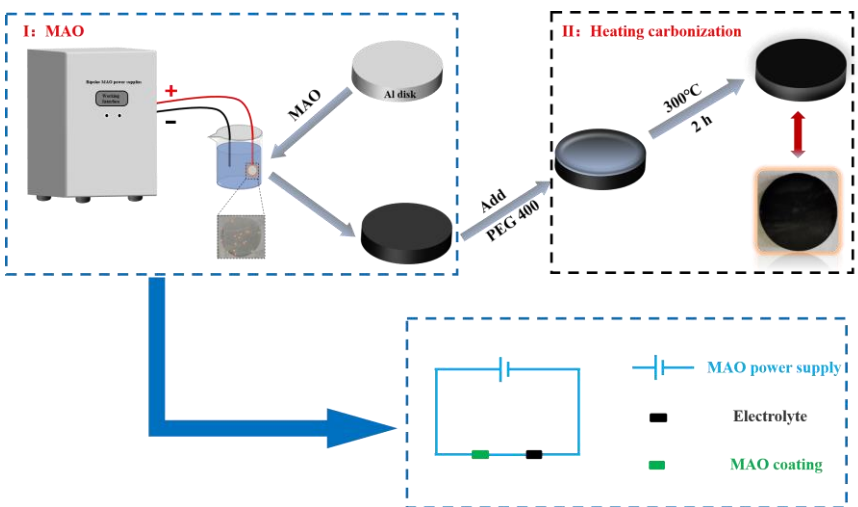

Fig. 1. The composite coating preparation process.

2.3. Coating characterization

After sampling the deionized water and white oil with a micro-sampler (A124021, Shanghai Gaoge Industry & Trade Co., Ltd., China), 5 μL of the liquid sample was dropped on the coating surface each time. When the liquid stabilized on the coating surface, it was photographed by an optical microscope (A0-V128S, Shenzhen Aosi Microoptics Instrument Co., LTD, China), with its contact angle being measured by a protractor. Each group of experiments was repeated three times, with the experimental results being averaged. The tribological tests were performed by using a steel wool friction tester (GRS-2, Shenzhen Zhijia Instrument Co., LTD, China) which was combined with a tensile pressure sensor (DYLY-107S, Bengbu Kunlun Precision Measurement Sensor Co., LTD, China) to obtain the coefficient of friction (COF). The friction counterparts in the tests were the prepared coating disk (Φ30 mm) and a SUS304 ball (Φ9.525 mm, Hardness ≤ 210 HV). After wiping the friction counterparts in acetone, the ball slid against the disk at a speed of 2 cm/s for 30 min under a high load of 10 N at room temperature (25±2°C). After the tribological tests, the wear diameter of the ball was observed under the A0-V128S optical microscope, while the surface and the cross-section structure of the disk were observed by SEM and EDS (OXFORD instruments, UK) based on which the wear width measurement and the elemental analysis were performed respectively. Each group of tests was executed three times, with the analysis results being averaged. In addition, the crystal phase structure and the chemical composition of the prepared coating samples were examined by XRD (D8 Advance diffractometer, Bruker, Germany), and XPS (Escalab 250Xi, Thermo Fisher Scientific, USA) and EDS respectively. The surface roughness of Al substrate and three different coatings (i.e., single MAO, single carbonized and composite ones) was measured by a metal plane roughness detector (TR200, Changzhou Sanfeng Instrument Technology Co., Ltd., China). The hardness of single MAO and composite coatings was examined by Q10A+ (Qness, Austria) Vickers hardness tester.

3. Experimental Results and Discussions

3.1. SEM analysis of single MAO and composite coating surfaces

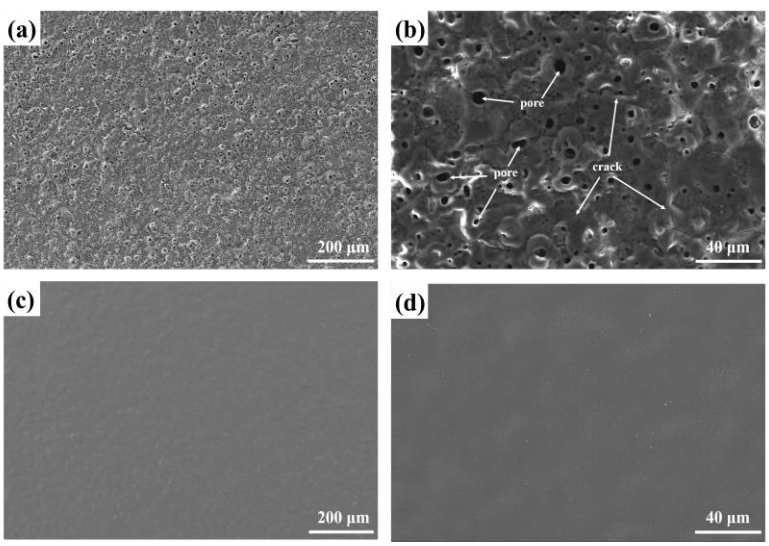

Fig. 2. (a) The SEM image and (b) partially enlarged image of single MAO coating surface, and (c) the SEM image and (d) partially enlarged image of composite coating surface.

Fig. 2 shows SEM images of single MAO and composite coating surfaces respectively. Due to the micro arcing generated in the discharge channel, the single MAO coating surface has many micropores (see Fig. 2(a)) which are one of the characteristics of most MAO coatings. Furthermore, the enlarged image Fig. 2(b) shows the dense volcano-like pores on the single MAO coating surface, accompanied by a large number of microcracks. This is caused by the similar cold extraction phenomena of the newly formed coating in electrolyte during the MAO process. [23, 24] Fig. 2(c) shows the surface morphology of the composite coating which clearly has a layer of dry material (i.e., the carbonized layer) attached onto the coating with some small bumps that are induced by the morphology of inner MAO coating. Compared to the single MAO coating in Fig. 2(b), the composite coating covered with a carbonized layer shows a smoother and flatter surface (see Fig. 2(d)).

3.2. EDS analysis of single MAO and composite coating surfaces

3.2.1. Single MAO coating surface

Fig. 3 shows the SEM image, EDS element scale and mapping images of single MAO coating surface. As shown in Fig. 3(b), the MAO coating mainly comprises O and Al elements with the contents of around 35.8% and 28.9% respectively. The content ratio between O and Al is around 3: 2, meaning that the MAO coating is mainly composed of Al_2O_3. The element mapping images in Figs. 3(c)-3(j) also show that O and Al are the main elements of MAO coating and that the remaining elements are low in content, most of which come from the components of the electrolyte.

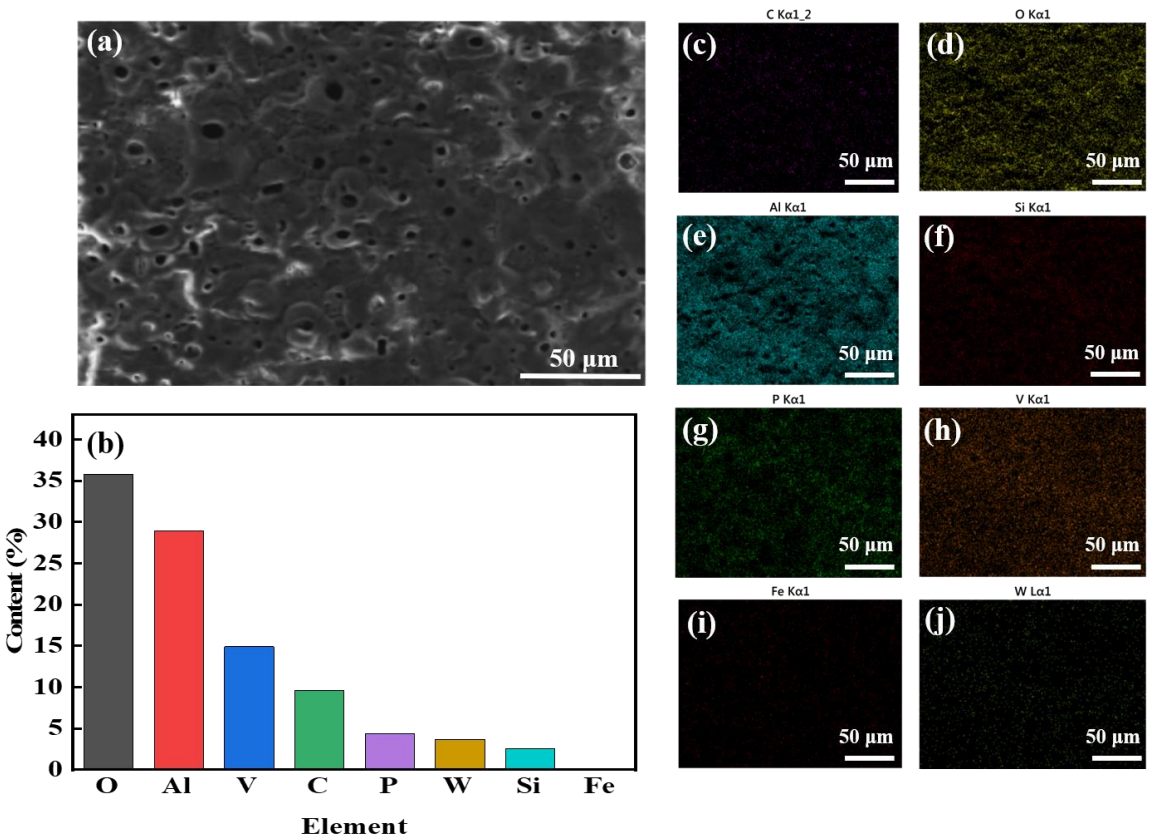

Fig. 3. (a) The SEM image, (b) EDS element scale image, and (c)-(j) element mapping images of single MAO coating surface.

3.2.2. Composite coating surface

Fig. 4 shows the SEM image, element scale and mapping images of the composite coating surface. As shown in Fig. 4(b), the carbonized layer on the composite coating surface is mainly composed of elements C and O, which are the two main elements contained in PEG 400 and account for around 66.7% and 33% of the total surface content respectively. The element mapping images in Figs. 4(c)-4(j) also show that C and O are the main elements in the composite coating surface. In addition, a number of residual trace elements are detected in the carbonized layer, which may be due to the uneven thickness of the carbonized layer.

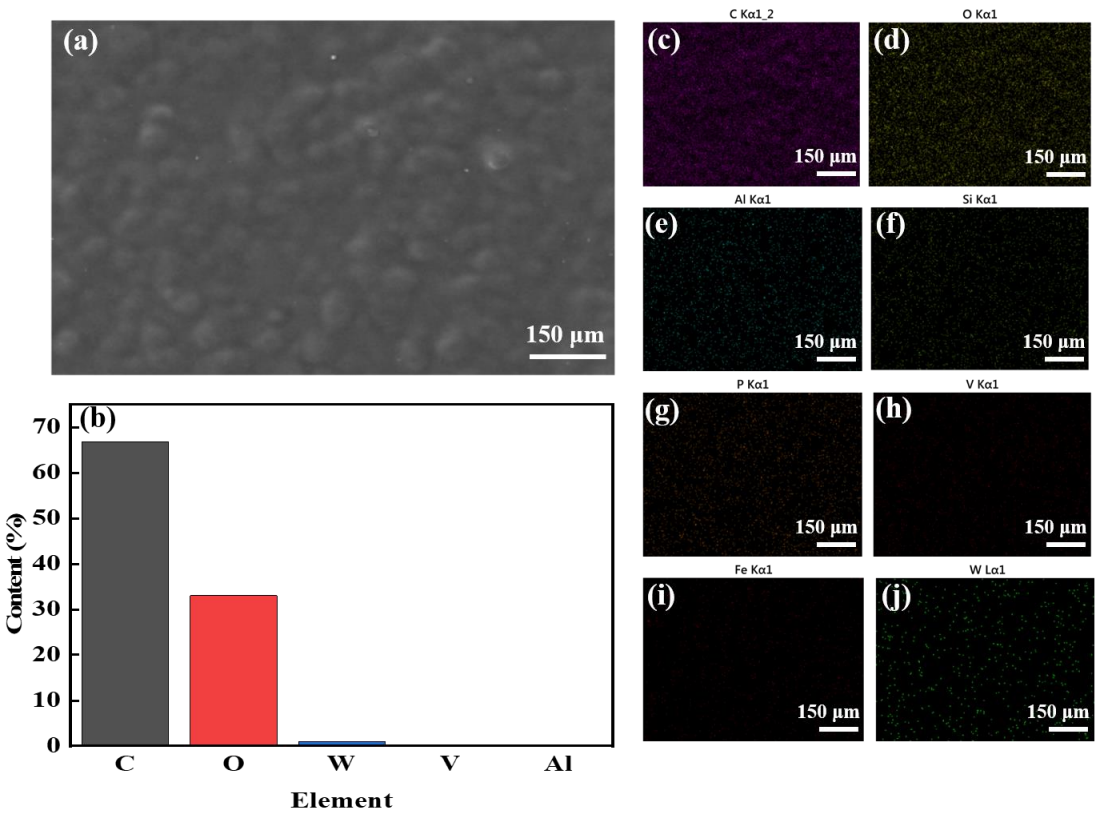

Fig. 4. (a) The SEM image (b) EDS element scale image, and (c)-(j) element mapping images of composite coating surface.

3.3. SEM and EDS analysis of cross section of composite coating

Fig. 5(a) provides a cross-sectional view of the composite coating which has a thickness of around 19.5 μm. The MAO coating within the composite coating exhibits an obvious accumulation of molten metal oxide and occupies a large thickness in the composite coating. The EDS scanning images of the cross section in Figs. 5(b)-5(i) show the main elements of C, O, Al, Si, P and V, as well as the trace elements of Fe and W, which are consistent with the EDS element analysis performed for single MAO and composite coating surfaces. The element C and part of O in the cross section come from the carbonized layer, while the rest elements are from the inner MAO coating. According to element mapping images of Al, Si, P and V that belong to the MAO coating only, it can be inferred that the thickness of inner MAO coating is around 17.5 μm, and thus the thickness of the carbonized layer is around 2 μm.

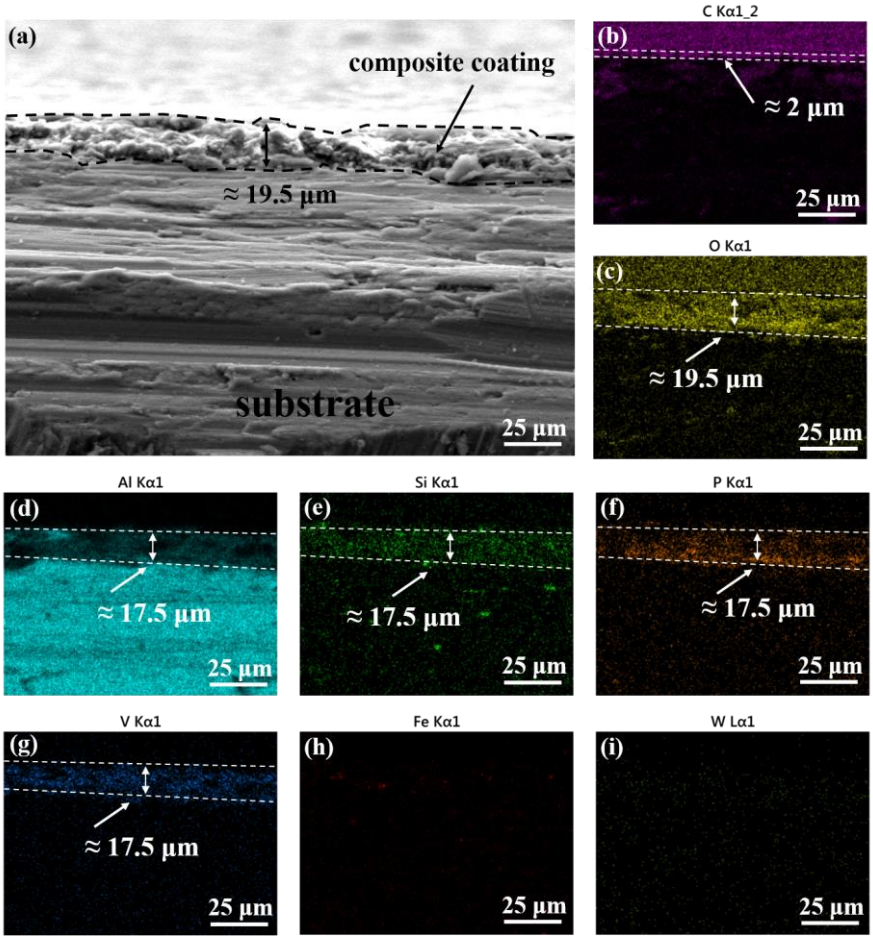

Fig. 5. (a) The SEM image and (b)-(i) element mapping images of cross section of composite coating.

3.4. XRD, contact angle, surface roughness and hardness analysis

The XRD images of single MAO and composite coatings are shown in Fig. 6(a) respectively where Al, α-Al_2O_3 and γ-Al_2O_3 are detected in both coatings, with the diffraction peak intensity of Al being much greater than those of α-Al_2O_3 and γ-Al_2O_3. According to the existing literature, the metastable γ-Al_2O_3 which mainly composes the loose outer layer can be converted into the stable α-Al_2O_3 which mainly makes up the dense inner layer at high temperature. [18, 25, 26] In addition, the overall XRD pattern of the composite coating is very similar to that of the single MAO coating, which might be due to the fact that the liquid PEG 400 did not crystallize or had poor crystallinity during the carbonization at 300°C. However, the diffraction peak intensity of Al in the composite coating is lower than that of the single MAO coating since the carbonized layer on the composite coating surface blocks the penetration of X-rays into Al substrate. [27]

Fig. 6(b) shows the contact angle test results for Al substrate and three different coatings. The contact angles of water and oil are less than 90° for all coatings, proving that they have hydrophilicity and lipophilicity. In particular, water and oil have smaller contact angles on the MAO coating, which may be due to the existence of volcano-like pores on the MAO coating surface. Since the carbonized layer of the composite coating covers the volcano-like pore structure of inner MAO coating, the hydrophilicity and lipophilicity of the composite coating are lower than the MAO coating and similar to the properties of the PEG 400 coating directly carbonized on Al substrate.

The surface roughness and hardness results of Al substrate and three different coatings are compared in Fig. 6(c). The surface roughness of the polished Al substrate is the smallest, while the single MAO coating has the largest surface roughness due to the existence of volcano-like pores and cracks on its surface. Since the carbonized layer of the composite coating fills and covers the volcano-like pores and cracks of the inner MAO coating (see Fig. 2), the composite coating has a smaller surface roughness than the single MAO coating. In addition, the single MAO coating is shown to have the highest hardness of around 302.7 HV due to the formation of hard α-Al_2O_3 and γ-Al_2O_3 crystal phases on the pure Al surface (see Fig. 6(a)). Compared to the single MAO coating, the outer PEG-carbonized layer of the composite coating reduces the surface hardness to around 144.16 HV, which might be due to the low hardness of the carbonized layer itself. However, the composite coating still exhibits a greater hardness than the pure Al substrate.

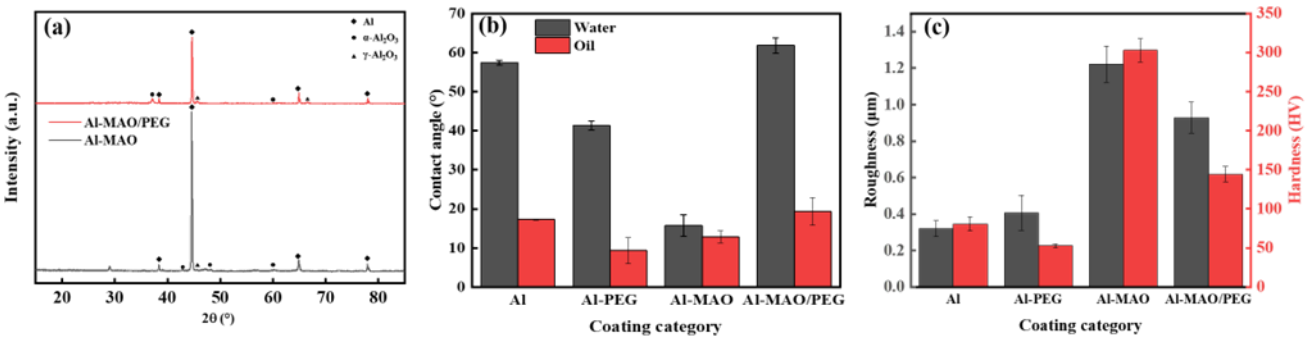

Fig. 6. (a) The XRD images of single MAO and composite coatings, (b) contact angle tests and (c) surface roughness and hardness tests of Al substrate and three different coatings.

3.5. XPS analysis of single MAO and composite coating surfaces

The XPS curves of single MAO and composite coating surfaces are shown in Fig. 7 respectively. It can be seen from Fig. 7(a) that the MAO coating mainly contains elements Na, O, C, Si, V, Al and P, and from Fig. 7(e) that the composite coating surface mainly contains elements C and O. Compared with the single MAO coating, the content of C element in the composite coating surface is obviously increased mainly due to the dense PEG-carbonized layer attached onto the composite coating surface. The element C in the MAO coating mainly exists in the form C-O-Al at 283.7 eV and C-O at 286.5 eV (see Fig. 7(b)), which may be due to the presence of PEG 4000 in the electrolyte, while the element C in the composite coating surface exists in the form of C-C at 283.5 eV, C-H at 284.6 eV and C-O at 287.3 eV (see Fig. 7(f)), which are the main forms of C in the carbonized layer of the composite coating. [28] Fig. 7(c) shows that the O element in the MAO coating mainly exists in the form of Al_2O_3 at 530.6 eV, followed by -OH and PO_3^-. [29] This means that $(NaPO_3)_6$ and less PEG in the electrolyte are introduced into the MAO coating. In the composite coating surface, the O element mainly exists in the form of C-O at 532.3 eV and -OH at 530.7 eV (see Fig. 7(g)), which is attributed to the PEG-carbonized layer on the surface. [28] Fig. 7(d) shows that the Al element in the MAO coating mainly exists in the form of Al_2O_3, while Fig. 7(h) does no detect the Al element in the composite coating surface, which is mainly because the inner MAO coating is well covered by the PEG-carbonized layer (see Fig. 2).

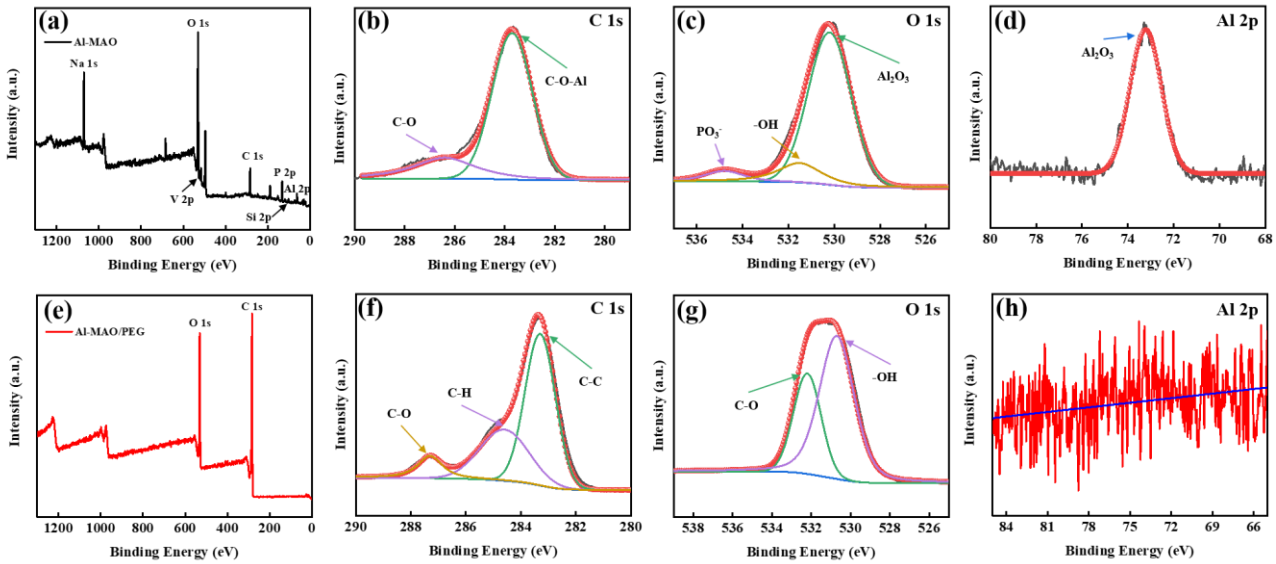

Fig. 7. The XPS of single MAO coating surface (a) survey, (b) C 1s, (C) O 1s and (d) Al 2p, and the XPS of composite coating surface (e) survey, (f) C 1S, (g) O 1S and (h) Al 2p.

3.6. Wear resistance analysis

3.6.1. Coefficient of Friction (COF)

Fig. 8(a) shows the COF curves during the sliding friction on pure Al and three different coatings under dry conditions. The unstable COF curve of pure Al has a high initial value, which is mainly due to the convex body contact between friction counterparts at the initial stage of sliding friction where the real contact area is much smaller than the theoretical contact area. According to the Hertzian contact theory, this increases the pressure at the contact point and the shear force in the process of reciprocating motion, resulting in higher COFs. Then the COF curve gradually decreases with time due to that the wear debris produced from the severe abrasive wear of the contact surface at the initial stage fill the uneven contact surface, increasing the contact area between friction counterparts and reducing the shear force in the process of reciprocal movement. The COF curve at the final stage of the sliding friction is generally stable but still fluctuates, which might be due to the adhesive wear between friction counterparts. The COF curve of the single PEG-carbonized coating is very low at the beginning of the sliding friction but rises considerably within a short period mainly due to the breakage of the coating. Then the COF curve fluctuations are reduced probably due to the wear debris from the PEG-carbonized coating breakage filling the uneven contact surface and increasing the contact area between friction counterparts. It is noted that the low stiffness of the single PEG-carbonized coating also slightly reduces the shear force on the coating surface, which appropriately mitigates the abrasive wear phenomena between friction counterparts and accordingly alleviates the adhesive wear phenomena. The COF curve of the single MAO coating shows the same trend as the curve of the pure Al at initial and middle stages, probably due to their similar wear conditions, but are smoother at the later stage of sliding friction, probably due to the high hardness and brittleness of wear debris which are less likely to induce adhesive wear between friction counterparts. Since the composite coating has a carbonized layer on the surface, its associated COF curve is similar to that of the single PEG-carbonized coating at the initial stage, and then

similar to that of the MAO coating at the later stage where the carbonized layer breakage might have occurred. In general, the composite coating exhibits a smoother COF curve during the sliding friction process with the occurrence of slight abrasive wear and oxidation wear and the alleviation of adhesion wear phenomena.

Fig. 8(b) shows wear widths of disks and wear diameters of balls after sliding friction experiments. The PEG carbonization on Al substrate and MAO coating is shown to reduce the wear of ball and disk to varying degrees, which might be due to the increasing surface smoothness. [30, 31] Furthermore, the existence of the composite coating results in the least wear on disk and ball. The wear width of the disk in the case of the composite coating is around 55.7%, 50.4% and 58.2% smaller than those in the cases of pure Al, single PEG-carbonized and single MAO coatings respectively, while the corresponding reductions in the wear diameter of the ball are around 55.2%, 47.8% and 60.4% respectively.

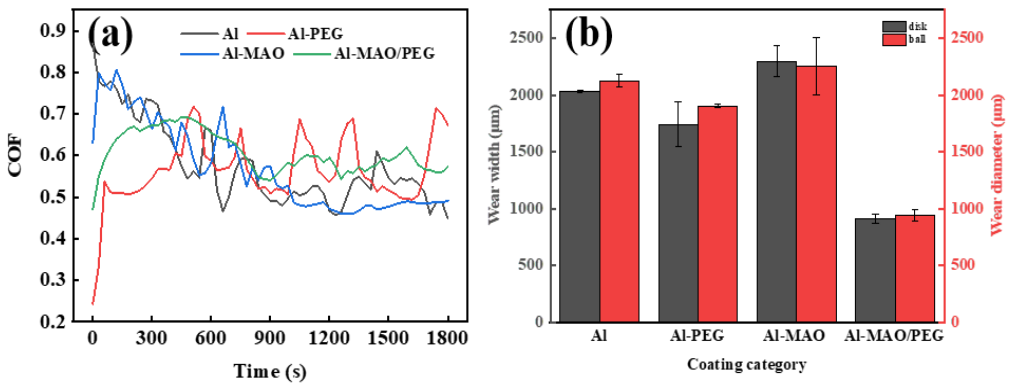

Fig. 8. (a) COF curves and (b) wear widths of disks and wear diameters of balls based on pure Al and three different coatings under dry friction.

3.6.2. Wear of disk

Figs. 9(a)-(d) show the light microscopic images of the wear of disks after sliding friction experiments based on pure Al and three different coatings respectively. The pure Al disk surface shows wide and deep furrows with a large number of adhesion points and some black spots which indicate that the pure Al substrate is worn out during sliding friction and thus oxidized and has a wear width of around 2031.6 μm (see Fig. 8(b)). This illustrates that the pure Al disk surface has severe abrasive wear and adhesive wear. The wide and deep furrows along with a small number of black points and adhesion points also appear on the single PEG-carbonized coating surface (see Fig. 9(b)), which means that the PEG-carbonized coating formed on Al substrate is broken during sliding friction. Compared with the pure Al disk in Fig. 9(a), the single PEG-carbonized coating significantly reduces the areas of black spots and adhesion points and slightly mitigates the wear of the disk which has a width of around 1742.4 μm (see Fig. 8(b)). This illustrates that the severe abrasive wear occurs on the surface of the PEG-carbonized Al disk, though the adhesive wear is mitigated. Fig. 9(c) shows that the ball breaks part of the single MAO coating and leaves wide and deep plough grooves on the inner pure Al substrate, causing a wear width of around 2298.1 μm on the disk (see Fig. 8(b)). The worn area also has a small number of sticking points, which indicates the occurrence of severe abrasive wear and slight adhesive wear on the surface of single MAO coating. Fig. 9(d) shows that the composite coating does not break down completely, though the lighter area indicates the breakage of the PEG-carbonized layer to some extent. The composite coating effectively alleviates both abrasive and adhesive wear on the disk, reducing

the wear width to 909.6 μm (see Fig. 8(b)) which is 55.2% smaller than the wear width of pure Al disk. This is probably due to the relatively smooth composite coating surface, the debris of abrasive wear further filling the composite coating surface and the lubricating effect of the carbonized PEG. The wear resistance experiments illustrate that the composite coating provides excellent wear resistance under dry friction, while the other two single coatings are broken to different degrees, leading to the severe wear on the pure Al substrate.

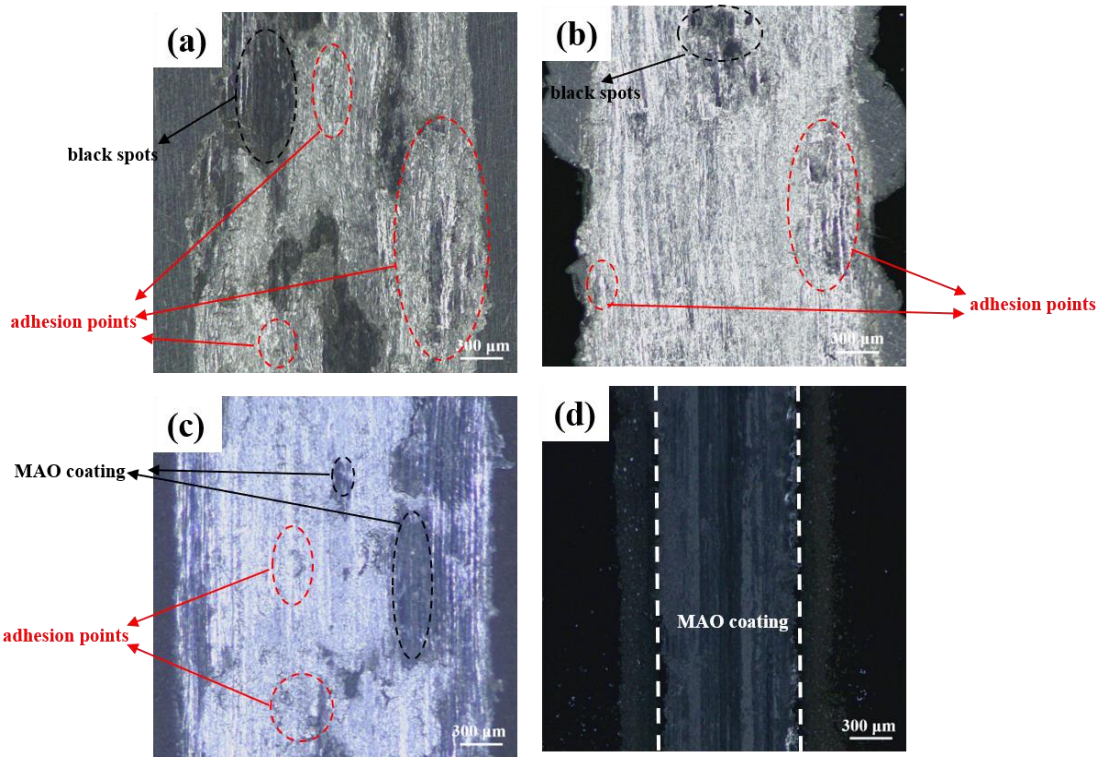

Fig. 9. Photomicrographs of disks under dry friction: (a) Al, (b) Al-PEG, (c) Al-MAO, (d) Al-MAO/PEG.

3.6.3. Wear of ball

Fig. 10 shows wear diameters of the balls that slid against pure Al and three different coatings under dry friction. The ball sliding against the composite coating has the smallest wear diameter of 982.696 μm, with shallow wear scratches on its surface (see Fig. 10(d)). In the cases of pure Al and single PEG-carbonized coating, the balls are shown to suffer from severe wear with wear diameters of 2209.774 μm and 1912.642 μm respectively (see Figs. 10(a) and 10(b)). Fig. 10(c) shows that the ball sliding against the single MAO coating has an elliptical wear shape, while others have approximately circular wear shapes. This may be because the severe abrasive wear of the single MAO coating creates a large amount of wear debris during the friction process, which accumulate at both ends of the wear track and provide high hardness. The wear debris at the wear track move relative to the ball, resulting in an elliptical wear shape on the ball.

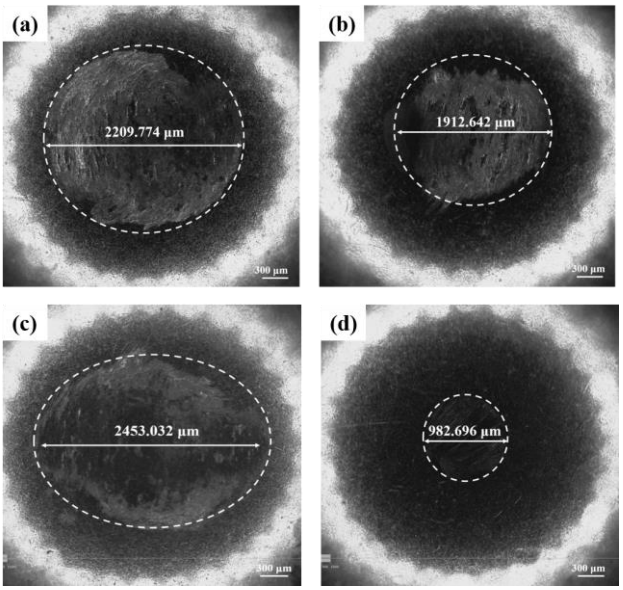

Fig. 10. Photomicrographs of balls under dry friction against (a) Al, (b) Al-PEG, (c) Al-MAO and (d) Al-MAO/PEG disks.

3.7. EDS element analysis of wear track on single MAO and composite coatings

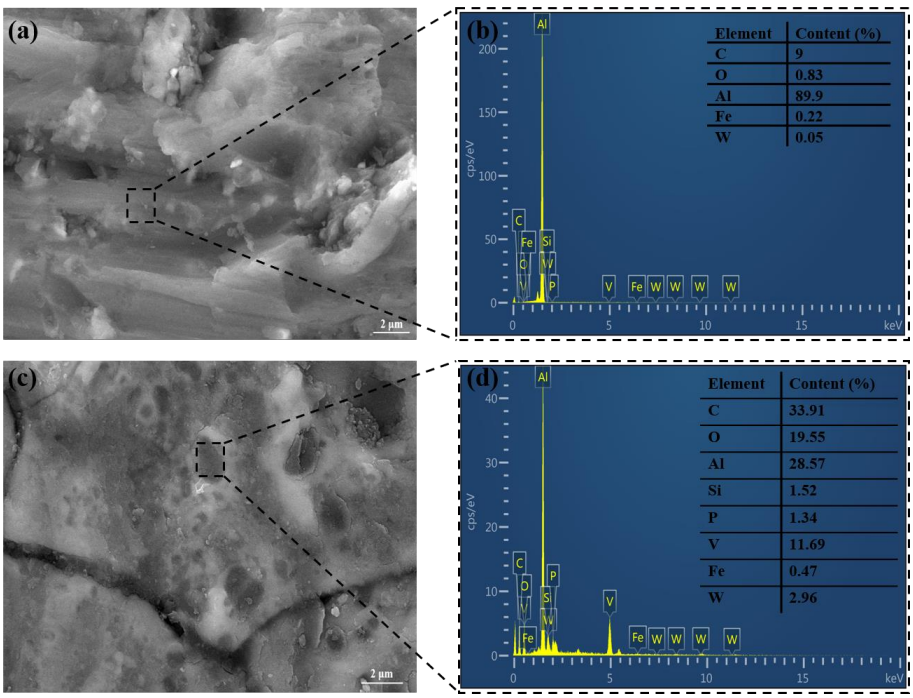

Fig. 11. The SEM images of wear track on (a) single MAO and (c) composite coatings, and the EDS element analysis of wear track on (b) single MAO and (d) composite coatings.

Fig. 11 shows the surface morphology and the EDS elemental analysis of single MAO and composite coatings with wear respectively. The single MAO coating has a large number of wear debris at the wear track (see Fig. 11(a)) which indicate the occurrence of severe abrasive

wear and adhesive wear. The corresponding EDS image in Fig. 11(b) shows that the content of Al element at the wear track reaches 89.9% which is much higher than the Al content of 28.9% in the original MAO coating, meaning that the complete breakage of the MAO coating at the wear track causes the direct exposure of inner Al substrate. Fig. 11(c) shows that the carbonized layer of the composite coating well fills the volcano-like pores and cracks of the inner MAO coating and alleviates the abrasive and adhesive wear on the composite coating surface, reducing wear debris on the coating surface. In addition, the content of element C at the wear track on the composite coating is 33.91% (see Fig. 11(d)) which is around half of the C content in the original composite coating (i.e., 66.7% as shown in Fig. 4(b)), indicating the loss of carbonized layer on the composite coating surface during sliding friction.

3.8. Comprehensive wear resistance of composite coating

3.8.1. Wear resistance analysis at different speeds

In order to verify the comprehensive wear resistance of the composite coating, the sliding friction experiments were carried out at different speeds with a load of 10 N for 30 min under dry environment. Fig. 12(a) compares the COF curves obtained at different speeds which are generally consistent with time, though the initial COF growth is mainly caused by the relatively severe abrasive wear. Furthermore, the COFs are shown to gradually decline with an increasing speed, which is also reflected in their averages (see Fig. 12(b)). This might be because the wear debris would be pushed out of the direct contact zone under the high-speed sliding friction, thus reducing the three-body wear and the COF between friction counterparts. In addition, the speed increase generally aggravates the wear on both composite coatings and balls, as shown in Figs. 12(c) and 12(d) respectively. It can be concluded that the composite coating has a low COF at the high-speed sliding friction under high load which will benefit the wear of the composite coating in short term, while the low-speed friction under high load will benefit the wear of the composite coating in long term.

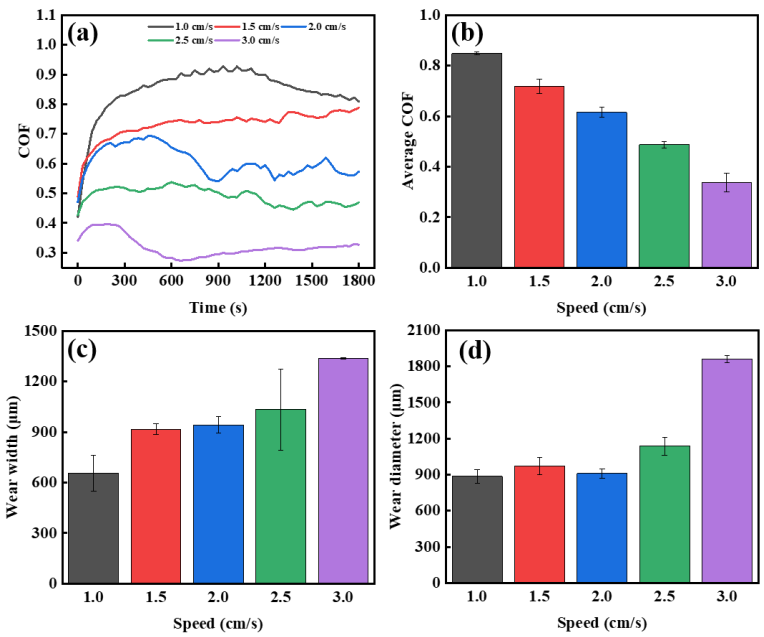

Fig. 12. (a) COF curves, (b) average COFs, (c) wear widths of disks and (d) wear diameters of balls sliding against the composite coating at different speeds.

3.8.2. Effects of lubricating mediums

To investigate the effects of lubricating mediums on the wear resistance of composite coating, the sliding friction experiments were carried out at a speed of 2 cm/s with a load of 10 N for 30 min under water and oil lubrication respectively. The COF curves recorded under the two lubrication conditions and their averages are compared in Figs. 13(a) and 13(b) respectively. Although the two lubrication mediums result in very similar COFs on average, the two COF curves have an obvious difference during the first 300 s where the COFs under oil lubrication are more stable than those that show a linear rise under water lubrication. This may be because the hydrophilicity of the composite coating is increased with the cracking of the carbonized layer under water lubrication, while the oil lubrication relatively mitigates the cracking of the carbonized layer. Figs. 13(c) and 13(d) show the wear widths of the composite coatings and the wear diameters of their corresponding balls which are very close under the lubrication effects of the two mediums. However, compared with the dry friction, the existence of water or oil lubrication reduces the COF but increases the wear degree of the composite coating, which might be due to the relatively good hydrophilicity and lipophilicity of the composite coating. Therefore, the composite coating provides better wear resistance in dry friction environment.

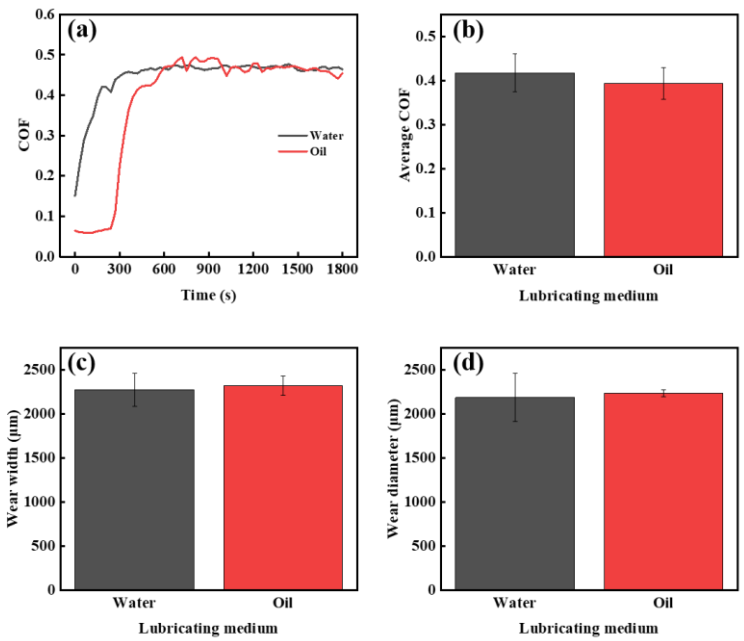

Fig. 13. (a) COF curves, (b) average COFs, (c) wear widths of disks and (d) wear diameters of balls sliding against the composite coating under water and oil lubrication.

3.9. Wear resisting mechanism

The wear resistance mechanisms of single MAO and composite coatings are shown in Fig. 14. The MAO coating consists of a dense inner layer mainly composed of α-Al_2O_3 and a loose outer layer mainly composed of γ-Al_2O_3. The outer layer of MAO coating has a large number of open holes and the inner layer has a proper number of closed holes, [32] resulting in a relatively rougher outer layer of the MAO coating. During the relative motion of the friction counterparts, their convex bodies are initially in contact with each other, and the shear force will produce large abrasive wear along with wear debris. Part of the wear debris will fill the uneven contact surface, while other debris stuck

between the two friction counterparts will cause adhesion wear during the reciprocal movement under high load. The thinner MAO coating will eventually wear off under high load due to large abrasive and adhesive wear, resulting in that the high-hardness wear debris cause more severe wear on the pure Al substrate. Compared with the single MAO coating, the carbonized layer of the composite coating not only fills the volcano-like holes and micropores of the inner MAO coating, forming a smoother coating surface, but also provides a certain lubricating effect. These helps alleviate the abrasive wear on the composite coating surface to some extent and reduce the production of wear debris at the beginning of the friction process. In addition, the reciprocating motion will increase the temperature of the contact surface, resulting in the occurrence of oxidation wear. [33] As with the single MAO coating, part of the wear debris fills the micropores of the composite coating surface, while part of them induce adhesive wear between friction counterparts. However, the composite coating mitigates the generation of wear debris and will not wear out completely, providing good protection for the pure Al substrate inside.

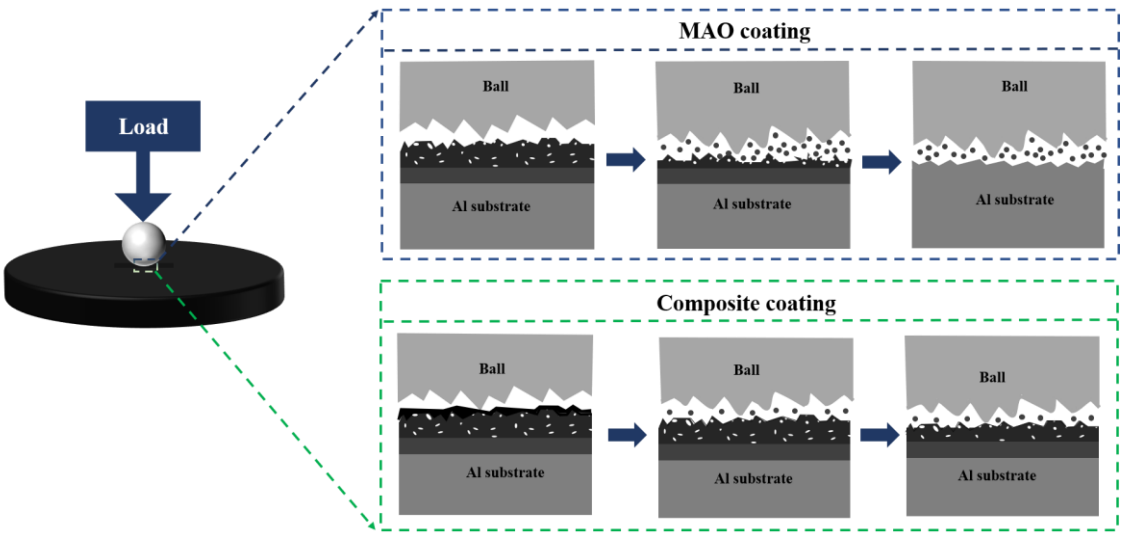

Fig. 14. Wear resisting mechanisms of single MAO and composite coatings.

4. Conclusions

In this paper, a new composite coating has been prepared on the surface of pure aluminum (Al) through a combination of the micro-arc oxidation (MAO) technology and the polyethylene glycol (PEG 400) carbonization technology. The composite coating and the single MAO coating have been observed by scanning electron microscope (SEM) and energy-dispersive spectrometer (EDS), which found that the MAO coating surface had volcano-like pores and microcracks and was well covered by the PEG-carbonized layer of the composite coating. The thickness of the composite coating prepared in this work was around 19.5 μm, of which the inner MAO coating thickness was about 17.5 μm. The material properties of the composite coating have been characterized by X-ray diffraction (XRD) and X-ray photoelectron spectroscopy (XPS). The MAO coating forming the inner layer of the composite coating comprised a loose outer layer mainly composed of metastable γ-Al_2O_3 and a dense inner layer mainly composed of stable α-Al_2O_3. The wear resistance of the composite coating has been also examined by tribological tests with a load of 10 N under different lubrication conditions. Compared with the pure Al substrate, single PEG-carbonized and

single MAO coatings, the application of the composite coating has reduced the surface wear width by around 55.7%, 50.4% and 58.2% respectively under dry friction environment, effectively mitigating abrasive wear and adhesive wear. In addition, the wear resistance of the composite coating has varied with the sliding speed under high load. Compared with the water and oil lubrication, the composite coating has exhibited a better wear resistance under dry environment. The composite coating technology which can provide good wear resistance for Al substrate has good application prospects.

Acknowledgement

This work was supported by Institute for Energy and Environment, University of Strathclyde.

Author contribution

Lu Chen and Zhonglei Shao developed the initial concept, wrote the initial paper and provided assistance for data acquisition and analysis. Fulin Fan revised the paper. All authors discussed the results and commented on the paper.

Conflict of interest

The authors declare that they have no known competing financial interests or personal relationships that could have appeared to influence the work reported in this paper.

References

1. Turan, M. E.; Aydin, F., Improved elevated temperature mechanical properties of graphene-reinforced pure aluminium matrix composites. *Materials Science and Technology* **2020,** *36* (10), 1092-1103.
2. Sercombe, T. B.; Schaffer, G. B., Rapid manufacturing of aluminum components. *Science (New York, N.Y.)* **2003,** *301* (5637), 1225-7.
3. Demirbas, C.; Ayday, A., Effect of Ag concentration on structure and wear behaviour of coatings formed by micro-arc oxidation on Ti6Al4 V Alloy. *Surface Engineering* **2021,** *37* (1), 24-31.
4. Wang, S.-P.; Zhou, L.; Li, C.-J.; Li, Z.-X.; Li, H.-Z.; Yang, L.-J., Morphology of composite coatings formed on Mo1 substrate using hot-dip aluminising and micro-arc oxidation techniques. *Applied Surface Science* **2020,** *508*.
5. Wu, G.; Wang, Y.; Sun, M.; Zhang, Q.; Yao, J.; Kovalenko, V., Effect of laser surface melting pretreatment on the growth behavior and mechanical properties of microarc oxidation coating on Ti6Al4V alloy. *Journal of Laser Applications* **2020,** *32* (1).
6. Hua, L.; Liu, J.; Li, S.; Yu, M., Effect of Adipic Acid on DEIS Characteristics during the Aluminium Anodizing Process in Sulfuric Acid Bath. *International Journal of Electrochemical Science* **2015,** *10* (3), 2194-2205.
7. Jariyaboon, M.; Moller, P.; Dunin-Borkowski, R. E.; Ambat, R., FIB-SEM investigation of trapped intermetallic particles in anodic oxide films on AA1050 aluminium. *Anti-Corrosion Methods and Materials* **2011,** *58* (4), 173-178.
8. Lameche-Djeghaba, S.; Benchettara, A.; Kellou, F.; Ji, V., Electrochemical Behaviour of Pure Aluminium and Al-5%Zn Alloy in 3% NaCl Solution. *Arabian Journal for Science and Engineering* **2014,** *39* (1), 113-122.
9. Lee, S.-J.; Kim, S.-J., Essential anti-corrosive behavior of anodized Al alloy by applied current density. *Applied Surface Science* **2019,** *481*, 637-641.
10. Tolochko, O. V.; Koltsova, T. S.; Bobrynina, E. V.; Rudskoy, A. I.; Zemtsova, E. G.; Kirichenko, S. O.; Smirnov, V. M., Conditions for Production of Composite Material Based on Aluminum and Carbon Nanofibers and Its Physic-Mechanical Properties. *Nanomaterials* **2019,** *9* (4).
11. Heinrichs, J.; Mikado, H.; Wiklund, U.; Jacobson, S., Wear of uncoated and PVD coated cemented carbide tools for processing of copper based materials part II: Exploring the sliding contact with pure copper. *Wear* **2021,** *466*.
12. Nagy, P.; Rohbeck, N.; Roussely, G.; Sortais, P.; Labar, J. L.; Gubicza, J.; Michler, J.; Pethoe, L., Processing and characterization of a multibeam sputtered nanocrystalline CoCrFeNi high-entropy alloy film. *Surface & Coatings Technology* **2020,** *386*.
13. Luo, Y.; Sun, Y.; Gu, Y.; Zhao, J.; Liang, J.; Yue, W., Enhanced Tribological Performance of a Ni/GO-Coated 2024 Alloy. *Journal of Materials Engineering and Performance* **2020,** *29* (5), 2947-2956.
14. Shadi, S.; Khabbazi, N. S.; Tabrizi, A. T.; Aghajani, H., Enhancing the Electroplated Chromium Coating for Corrosion Protection of Aluminum by Adding Graphene Oxide. *Surface Engineering and Applied Electrochemistry* **2022,** *58* (2), 202-209.
15. Li, C.; Lu, H.; Xu, G.; Hu, F.; Li, J.; Wang, L., Flexible graphene oxide/poly(ethylene glycol) composite films for lubrication application. *Materials Chemistry and Physics* **2022,** *277*.

16. Li, C.; Xu, G.; Wang, L.; Li, J.; Lu, H., Tribological properties of graphene oxide and polyethylene glycol composites under dry friction and oil lubrication conditions. *Journal of Applied Polymer Science* **2022,** *139* (15).
17. Li, K.; Li, Q., Research and application progress of micro-arc oxidation on the alloys. *Rare Metal Materials and Engineering* **2007,** *36*, 199-203.
18. Zhang, K.; Yu, S., Preparation of wear and corrosion resistant micro-arc oxidation coating on 7N01 aluminum alloy. *Surface and Coatings Technology* **2020,** *388*.
19. Yang, W.; Li, Q.; Liu, W.; Liang, J.; Peng, Z.; Liu, B., Characterization and properties of plasma electrolytic oxidation coating on low carbon steel fabricated from aluminate electrolyte. *Vacuum* **2017,** *144*, 207-216.
20. Cheng, Y.; Wu, F.; Dong, J.; Wu, X.; Xue, Z.; Matykina, E.; Skeldon, P.; Thompson, G. E., Comparison of plasma electrolytic oxidation of zirconium alloy in silicate- and aluminate-based electrolytes and wear properties of the resulting coatings. *Electrochimica Acta* **2012,** *85*, 25-32.
21. Molak, R. M.; Topolski, K.; Spychalski, M.; Dulinska-Molak, I.; Moronczyk, B.; Pakiela, Z.; Nieuzyla, L.; Mazurkiewicz, M.; Wojucki, M.; Gebeshuber, A.; Piotrowska, N., Functional properties of the novel hybrid coatings combined of the oxide and DLC layer as a protective coating for AZ91E magnesium alloy. *Surface & Coatings Technology* **2019,** *380*.
22. Liu, J. A.; Zheng, Z. B.; Li, J. Q.; Zhu, X. Y.; Liu, Y.; Bi, G. L., Effect of current density on structure and property of coloured coating on aluminium via micro-arc oxidation. *Materials Research Innovations* **2015,** *19*, S79-S82.
23. Guo, H. F.; An, M. Z., Growth of ceramic coatings on AZ91D magnesium alloys by micro-arc oxidation in aluminate-fluoride solutions and evaluation of corrosion resistance. *Applied Surface Science* **2005,** *246* (1-3), 229-238.
24. Duan, H. P.; Du, K. Q.; Yan, C. W.; Wang, F. H., Electrochemical corrosion behavior of composite coatings of sealed MAO film on magnesium alloy AZ91D. *Electrochimica Acta* **2006,** *51* (14), 2898-2908.
25. Yang, C.; Zhu, J.; Cui, S.; Chen, P.; Wu, Z.; Ma, Z.; Fu, R. K. Y.; Tian, X.; Chu, P. K.; Wu, Z., Wear and corrosion resistant coatings prepared on LY12 aluminum alloy by plasma electrolytic oxidation. *Surface and Coatings Technology* **2021,** *409*.
26. Li, Z.-y.; Cai, Z.-b.; Cui, Y.; Liu, J.-h.; Zhu, M.-h., Effect of oxidation time on the impact wear of micro-arc oxidation coating on aluminum alloy. *Wear* **2019,** *426-427*, 285-295.
27. Kaseem, M.; Ko, Y. G., Effect of starch on the corrosion behavior of Al-Mg-Si alloy processed by micro arc oxidation from an ecofriendly electrolyte system. *Bioelectrochemistry* **2019,** *128*, 133-139.
28. Chen, L.; Tu, N.; Wei, Q.; Liu, T.; Li, C.; Wang, W.; Li, J.; Lu, H., Inhibition of cold‐welding and adhesive wear occurring on surface of the 6061 aluminum alloy by graphene oxide/polyethylene glycol composite water‐based lubricant. *Surface and Interface Analysis* **2021,** *54* (3), 218-230.
29. Du, C.; Zhao, H.; Dai, Z.; Tian, Z.; Wang, J.; Wang, Z., The preparation and properties of black coating by micro arc oxidation on 2A12 aluminum alloy. *Materials Letters* **2019,** *236*, 723-726.
30. Tabrizi, A. T.; Aghajani, H.; Laleh, F. F., Tribological Study of Thin-Electroplated Chromium: Evaluation of Wear Rate as a Function of Surface Roughness. *Experimental Techniques* **2021**.
31. Tabrizi, A. T.; Aghajani, H.; Saghafian, H.; Laleh, F. F., Correction of Archard equation for wear behavior of modified pure titanium. *Tribology International* **2021,** *155*.
32. Malayoglu, U.; Tekin, K. C.; Shrestha, S., Influence of post-treatment on the corrosion resistance of PEO coated AM50B and AM60B Mg alloys. *Surface & Coatings Technology* **2010,** *205* (6), 1793-1798.
33. Tabrizi, A. T.; Aghajani, H.; Laleh, F. F., Tribological characterization of hybrid chromium nitride thin layer synthesized on titanium. *Surface & Coatings Technology* **2021,** *419*.